ANALYSIS OF WILLIAMSON NANOFLUID WITH VELOCITY AND THERMAL SLIPS PAST OVER A STRETCHING SHEET BY LOBATTO IIIA NUMERICALLY

by

Sharafat ALI[a], Muhammad Asif Zahoor RAJA[b,c], Tahir Nawaz CHEEMA[a], Iftikhar AHMAD[a*], Numan MIAN[a], and Muhammad SHOAIB[d]

[a] Department of Mathematics, University of Gujrat, Gujrat, Pakistan
[b] Future Technology Research Center, National Yunlin University of Science and Technology, Douliou, Yunlin, Taiwan
[c] Department of Electrical and Computer Engineering, COMSATS University Islamabad, Attock Campus, Attock, Pakistan
[d] Department of Mathematics, COMSATS University Islamabad, Attock Campus, Attock, Pakistan

Original scientific paper
https://doi.org/10.2298/TSCI200620159A

A novel numerical computing framework through Lobatto IIIA method is presented for the dynamical investigation of nanofluidic problem with Williamson fluid flow on a stretching sheet by considering the thermal slip and velocity. The impact of thermophoresis and Brownian motion on phenomena of heat transfer are explored by using Buongiorno model. The governing non-linear partial differential system representing the mathematical model of the Williamson fluid is transformed in to a system of ODE by incorporating the competency of non-dimensional similarity variables. The dynamics of the transformed system of ODE are evaluated through the Lobatto IIIA numerically. Sufficient graphical and numerical illustrations are portrayed in order to investigate and analyze the influence of physical parameters: Williamson parameter, Prandtl number, Lewis number, Schmidt number, ratio of diffusivity parameter, ratio of heat capacitance parameter on velocity, temperature, and concentration fields. The numerically computed values of local Nusselt number, local Sherwood number, and skin friction coefficient are also inspected for exhaustive assessment. Moreover, the accuracy, efficiency and stability of the proposed method is analyzed through relative errors.

Key words: *Williamson nanofluid, slip conditions, stretching sheet, heat transfer, Lobatto IIIA approach*

Introduction

Fluid mechanics is a well-known class of physical sciences which deals about the fluids behavior whether they are stationary or moving. It plays an essential role to measure the tornado vorticity, to model the Jupiter red spot, or analyzed the impact of subatomic particles in a betatron, *etc*. Moreover, it facilitates the base for combustion and propulsion, oceanography and meterology, for particle physics and biofluids, *etc*. The materials including polymer melts and natural products, biological fluids and agricultural waste, soap solutions, lavas, and magmas are exhibiting the characteristics of non-Newtonian fluid flows.

* Corresponding author, e-mail: dr.iftikhar@uog.edu.pk

Nanofluid is a special class of fluids which is composed of base fluid with nano-size particles. Diverse metals such as copper, silicon, and aluminum prescribed the nanoparticles. It is preliminary noted that the shape of the nanoparticles may be like spherical, rod-like and tubular. Basically, the nanoparticles are used in base fluid to enlarge the heat transfer characteristics such as thermal conductivity, radiation, and convection. The primary intent of nanofluids is to enlarge the thermal conductivity of the base fluids. There are numerous industrial and technological fields in which nanofluids mostly used are air conditioning, biomedicine, nuclear reactor, radiators, hybrid power engines, transportation, and chemical productions, *etc*.

The name of Williamson fluid has been introduced firstly by Williamson in 1929. He developed the mathematical equations of the Williamson fluid to investigate their flow properties and behavior along with the experimentally derived results [1]. The approach of boundary-layer flow dynamics was introduced by Prandtl in 1904. He explained the major differences between the inviscid and viscid flow using boundary layer approach [2]. The first study on flow of boundary-layers over a stretching sheet model was conducted by Sakiadis and his fellow in 1961 [3]. Further, the mathematical system of equations of boundary-layer flow involving Williamson nanofluid were formulated by [4]. The analysis of heat transport of Williamson nanofluid in the presence of thermal radiations and slip velocity have a abundan range of applications in production of glass-fibers and papers, production of polymer extrusion, copper wire drawing and in various plastic industries [5]. The slip condition is assumed in stretching sheet system of Williamson nanofluid flow because the existance of nanoparticles creates the links between solid boundary and fluid slip velocity [6]. Ahmad *et al.* [7] investigated the MHD bi-directional nanofluid flow past an exponentially stretching sheet. They concluded that exponent temperature parameter at surface of sheet is the prime factor which leads to enlarge the rate of heat transport. Bai *et al.* [8] analyzed the impacts of Maxwell nanofluids flow with diffusion parameter through a stretching surface using homotopy analysis method. Their consequences revealed that heat transport rate is a reducing function of thermophoresis. In other treatments [7], Patel model explore the properties of heat transfer with thermal radiations. They computed the numerical solution to the governing problems in computer software by utilizing famous Runge-Kutta-Fehlberg technique. A solar energy model was formulated for 3-D MHD flow of Jeffery nanofluid to investigate the effects of Brownian motion and thermophoresis, *etc.* [9]. Ibrahim [10] examined numerically the stagnation-point nanofluid flow for melting heat transport past a stretched sheet. Reddy *et al.* [11] found the numerical solution of Williamson nanofluid flow along with varying thermal conductivity and thickness past a stretching sheet by utilizing spectral quasi-linearization technique. The stagnation point flow with heat generation/aborption along with radiation effects through a moving wedge were studied in [12]. They utilized finite-difference solver to the governing equations for numerical results and concluded that radiation parameter upgrade the heat transport rate.

The heat transport of Sisko nanofluid with non-linear radiations through a stretching sheet were examined by [13]. They reported that velocity profile become decreasing by raising the Sisko parameter. Alam *et al.* [14] investigated the flow of MHD and unsteady nanofluid through a moving wedge. They found that stronger magnetic parameter raise the velocity profile. The numerical behavior of delay differential equation is also observed by using Lobatto IIIA procedure [15]. The Hamiltonian type PDE like non-linear Shero-dinger equation and non-linear wave equation are tackled numerically through an effective, and reliable computational solver known as Lobatto IIIA scheme [16]. Numerical solution of Sisko fluid involving nanomaterial by Lobatto IIIA solver [17]. Numerical analysis of mixed convection along with Navier slip velocity under activation energy for the flow of magnetonanomaterials model by Lobatto IIIA approach [17]. A reliable study of Lobatto IIIA solver in Darcy-Forchheimer model for carbon nano-tubes with rotating flow in 3-D [18]. Moreover, in 2021 era the different fluid dynamics model are numerically investigated through Lobatto IIIA including, nanofluidic model with mixed convection to investigate the effect of involved parameters in the velocities and temperature profiles [19], 3-D MHD-hybrid nanofluid flowing over the rotating disk along viscous dissipation and Joule heating effects in the presence of thermal radiation [20]. Furthermore, Al_2O_3-Cu-H_2O hybrid nanofluidic problem over the rotating with stretching/shrinking sheet is numerically studied through Lobatto IIIA solver under the effect of Darcy-Forchheimer porous medium [21], double dispersion equation [22], drug delivery system [23]. The salient features of the study are briefly highlighted as follows.

- A novel numerical investigation with Lobatto IIIA is introduced for the dynamical study of nanofludic Williamson flow on a stretching sheet considering velocity and thermal slips conditions.
- The primary concept of boundary-layer fluid flow model is incorporated to establish PDE of the dynamical system, and these PDE are transformed into relevant ODE by the competency of non-dimensional similarity variable approach.
- The application of Lobatto IIIA based finite difference numerical scheme to study the velocity, temperature and concentration profiles for different scenarios of nanofluidic Williamson flow model.
- Lobatto IIIA numerical scheme is exploited to compute the data of skin friction coefficient, local Nusselt, and Sherwood number for exhaustive analysis.

Modeling of flow equations

Consider the steady state and 2-D flow of incompressible Williamson fluid along with effect of velocity and thermal slips past through a stretching sheet are depicted in fig 1. In this fluidic model, $u_w = cx$ acts as a linear velocity on the surface of the sheet while the measured co-ordinate along the direction of stretched surface is denoted by x and c behave like a constant. The temperature of wall defined as $T_w = bx^2 + T_\infty$ in this model.

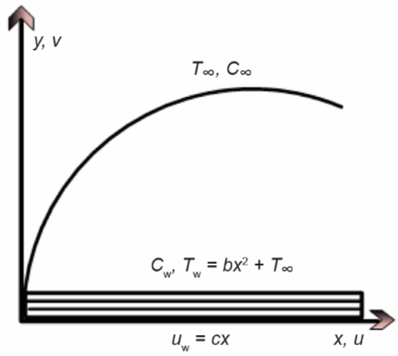

Figure 1. Geometry of physical flow

The governing fluidic time independent boundary-layer transport equations for stretching sheet geometry are given as:

$$\frac{\partial u}{\partial x} + \frac{\partial v}{\partial y} = 0 \tag{1}$$

$$u\frac{\partial u}{\partial x} + v\frac{\partial u}{\partial y} = \nu\frac{\partial^2 u}{\partial y^2} + \sqrt{2}\nu\Gamma^*\frac{\partial u}{\partial y}\frac{\partial^2 u}{\partial y^2} \tag{2}$$

$$u\frac{\partial T}{\partial x} + v\frac{\partial T}{\partial y} = D_B\frac{\partial T}{\partial y}\frac{\partial C}{\partial y}\frac{\rho C_p}{\rho C} + \beta\frac{\partial^2 T}{\partial y^2} + \frac{\rho C_p}{\rho C}\frac{D_T}{T_\infty}\left(\frac{\partial T}{\partial y}\right)^2 \tag{3}$$

$$u\frac{\partial C}{\partial x}+v\frac{\partial C}{\partial y}=\frac{D_T}{T_\infty}\frac{\partial^2 T}{\partial y^2}+D_B\frac{\partial^2 C}{\partial y^2} \tag{4}$$

The appropriated boundary conditions are:

$$u=u_\mathrm{w}+\delta\mu\left(\frac{\partial u}{\partial y}\right),\quad u_\mathrm{w}=cx,\quad v=0,\quad T=bx^2+T_\infty+\gamma\frac{\partial T}{\partial y}$$
$$C=C_\mathrm{w}\ \text{at}\ y=0,\quad u\to 0,\quad T\to T_\infty,\quad C=C_\infty\ \text{as}\ y\to\infty \tag{5}$$

The similarity variables are introduced:

$$u=cxf'(\eta),\quad v=-(cv)^{1/2},\quad \eta=\sqrt{\frac{c}{v}}y,\quad \theta=\frac{T-T_\infty}{T_\mathrm{w}-T_\infty},\quad \phi=\frac{C-C_\infty}{C_\mathrm{w}-C_\infty} \tag{6}$$

The non-dimensional coupled system of ODE for stretching sheet model after solving PDE of eqs. (2)-(4) by inserting transformations defined in (6) are:

$$f'''+\lambda f'''f''+f''f-f'^2=0 \tag{7}$$

$$\theta''+\Pr f\theta'-2\Pr f'\theta+\frac{Nc}{\mathrm{Le}}Nt\theta'^2+\frac{Nc}{\mathrm{Le}}\theta'\phi=0 \tag{8}$$

$$\phi''+\mathrm{Sc}\phi'f+\frac{1}{Nb}\theta''=0 \tag{9}$$

where velocity, temperature and concentration, f, θ, and ϕ depend of η, while the prime indicates differentiation of said independent variable η. After solving eqs. (5) and (6), the transformed boundary conditions are:

$$f(0)=0,\quad f'(0)=1+\delta f''(0),\quad \theta(0)=1+\gamma\theta'(0),\quad \phi(0)=1$$
$$\text{as}\ y=0,\quad f'(\infty)=1,\quad \theta(\infty)=1,\quad \phi(\infty)=1,\quad \text{as}\ \eta\to\infty \tag{10}$$

The fluidic physical parameters such as Williamson parameter, λ, Prandtl number, Lewis number, Schmidt number, ratio of diffusivity parameter, Nt, and ratio of heat capacitance parameter, Nc, are defined:

$$\lambda=\sqrt{\frac{2c^3}{\nu}}\Gamma^* x,\quad \Pr=\frac{\nu}{\beta},\quad \mathrm{Le}=\frac{\beta}{D_B},\quad \mathrm{Sc}=\frac{\nu}{D_B}$$
$$Nt=\frac{T_\infty D_B(C_\mathrm{w}-C_\infty)}{D_T(T_\mathrm{w}-T_\infty)},\quad Nc=\frac{\rho_p C_p}{\rho C}(C_\mathrm{w}-C_\infty) \tag{11}$$

The skin friction, Nusselt number, and Sherwood number are represented with $\bar{C}_f$, $\bar{\mathrm{N}}\mathrm{u}$, and $\bar{\mathrm{S}}\mathrm{h}$, respectively and are expressed:

$$\bar{C}_f=\frac{\tau_\mathrm{w}}{\rho u_\mathrm{w}^2},\quad \bar{\mathrm{N}}\mathrm{u}=\frac{xq_\mathrm{w}}{k^*(T_\mathrm{w}-T_\infty)},\quad \bar{\mathrm{S}}\mathrm{h}=\frac{xq_\mathrm{m}}{D_B(C_\mathrm{w}-C_\infty)} \tag{12}$$

where the shear stress, heat flux, and mass flux are denoted by τ_w, q_w, and q_m, respectively and are given:

$$\tau_w = \mu\left[\frac{\partial u}{\partial y} + \frac{\Gamma^*}{2}\left(\frac{\partial u}{\partial y}\right)^2\right], \quad q_w = -k^*\frac{\partial T}{\partial y}\bigg|_{y=0}, \quad q_m = -D_B\frac{\partial C}{\partial y}\bigg|_{y=0} \tag{13}$$

After solving eqs. (12) and (13) the most interesting dimensionless form of skin friction, local Nusselt, and Sherwood numbers becomes:

$$\bar{C}_f\sqrt{\text{Re}} = f''(0) + \frac{\lambda}{2}f''(0), \quad \frac{\text{Nu}}{\sqrt{\text{Re}}} = -\theta'(0), \quad \frac{\text{Sh}}{\sqrt{\text{Re}}} = -\phi'(0) \tag{14}$$

Results and discussion

The governing fluidic non-linear partial differential system of the Williamson fluidic model for stretching sheet geometry are altered into ordinary differential systems by utilizing similarity variables approach.

After that, the transformed coupled set of ODE eqs. (7)-(9) are handled numerically subject to the attached boundary conditions eq. (10) through Lobatto IIIA technique with the help of MATLAB routine bvp4c as per procedure shown in fig 2. The detail description of the proposed methodology is available in [24]. The action of physical fluidic parameters such as λ, Pr, Le, Sc, ratio of diffusivity parameter, Nt, and ratio of heat capacitance parameter, Nc, on dimensionless stream function $f(\eta)$, velocity field $f'(\eta)$, temperature field $\theta(\eta)$, and concentration field $\phi(\eta)$ are observed by plotting graphs. Table 1 illustrated the fluidic parameters Variation for the numerical simulation of Williamson fluidic system.

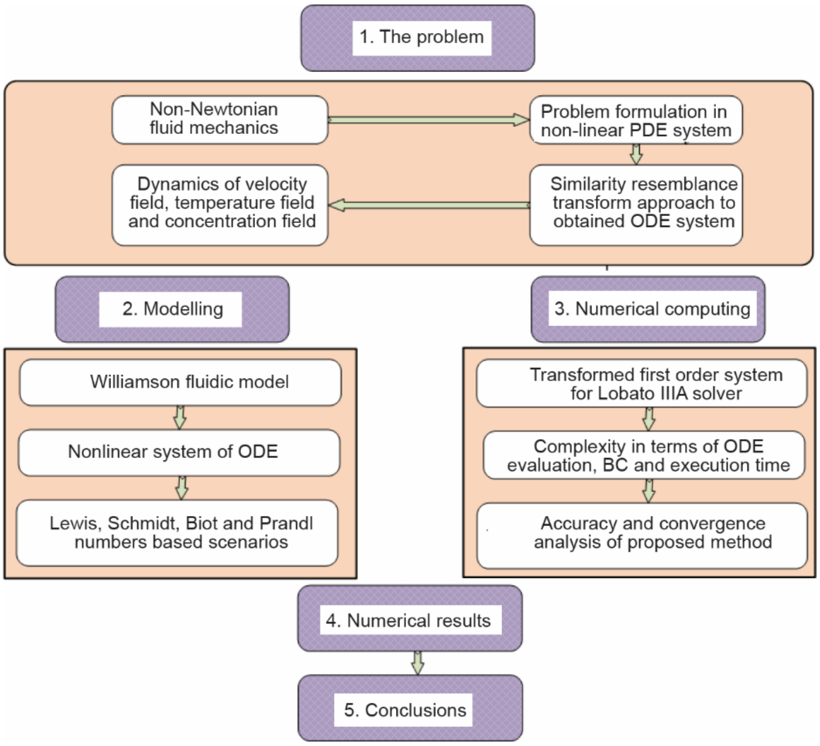

Figure 2. Working flow chart of fluidic model

Table 1. Parameters variation of the proposed model

Index	C-1	C-2	C-3	C-4
δ	0.4	0.8	1.2	1.6
γ	0.3	0.4	0.6	0.9
λ	1.0	1.5	2.0	2.5
Pr	0.0	0.4	0.8	1.2
Nc	0.2	0.4	0.6	0.8
Le	0.25	0.75	1.25	1.75
Nt	2.0	4.0	6.0	8.0
Sc	4.0	6.0	8.0	10

Table 2. Nusselt number analysis for proposed model

Index	C-1	C-2	C-3	C-4
δ	0.7687	0.7448	0.7280	0.7146
γ	1.9018	1.3796	1.0819	0.8897
λ	1.2228	1.2151	1.2038	1.1814
Pr	1.0557	1.1708	1.2038	1.3056
Nc	1.1850	1.1283	1.0709	1.0138
Le	0.8651	0.9820	1.0464	1.0860
Nt	0.0522	0.0626	0.0766	0.0887
Sc	1.2234	1.2157	1.2102	1.2059

Figures 3(a) and 3(b) elucidate the impact of *Nc* on f and f', respectively. The function f and f' depicted decreasing behavior by increasing *Nc*. Figures 3(c) and 3(d) render the impacts of *Nc* on θ and ϕ, respectively. The value of θ and ϕ increases by increasing *Nc*. Figure 3(e) narrated the effect of *Nt* on $\theta(\eta)$ and while fig. 3(f) portrays the effects of *Nt* on $\phi(\eta)$. The temperature profile θ is reducing while the concentration profile ϕ is increasing gradually for increased values of *Nt*. Figures 4(a) and 4(b) elaboratively present the actions of f and θ against η for different values of δ.

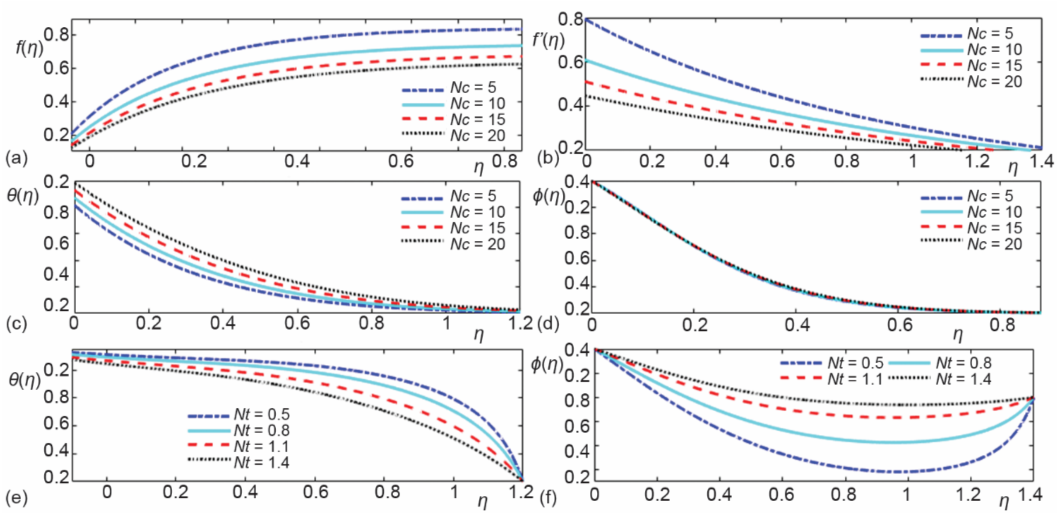

Figure 3. Impact of *Nc* on f, f', θ, and ϕ while of *Nt* on θ and ϕ; (a) f for *Nc* variation, (b) f' for *Nc* variation, (c) θ for *Nc* variation, (d) ϕ for *Nc* variation, (e) θ for *Nt* variation, and (f) ϕ for *Nt* variation
(*for color image see journal web site*)

Both f' and θ reduced by increasing δ. Figures 4(c) and 4(d) rendered the impacts of θ and f graphically for various values of δ. The results indicates that $\theta(\eta)$ and $\phi(\eta)$ increase by increment in value of δ.

Figures 4(e) and 4(f) illuminated the influence of Lewis number, on θ and ϕ, respectively. The temperature curve reducing all the time but concentration curve increase initially and after a certain limit, it become decreasing by enlargement in value of Le. Figures 5(a) and 5(b) demonstrate the action of f and f' for distinct values of λ. The results clarify that curves of f and f' gone downward for increasing value of λ. The consequences of λ on θ and ϕ are depicted in figs. 5(c) and 5(d), respectively. The values of $f(\eta)$ and $f'(\eta)$ significantly boosts with increment in λ. Figures 5(e) and 5(f) display the consequences of θ and ϕ for η by taking sundry values of Schmidt number, respectively. The $\theta(\eta)$ increases while $\phi(\eta)$ decreases for increment in the values of Schmidt number. Figures 6(a) and 6(b) demonstrate the impacts of γ on f and θ, respectively. Both f and ϕ decrease by increasing γ. The impact of Prandtl number on f, θ, and ϕ are shown graphically in figs. 6(d)-6(f), respectively. The increment in magnitude of Prandtl number leads to dropped the value of all three f, θ, and ϕ profiles.

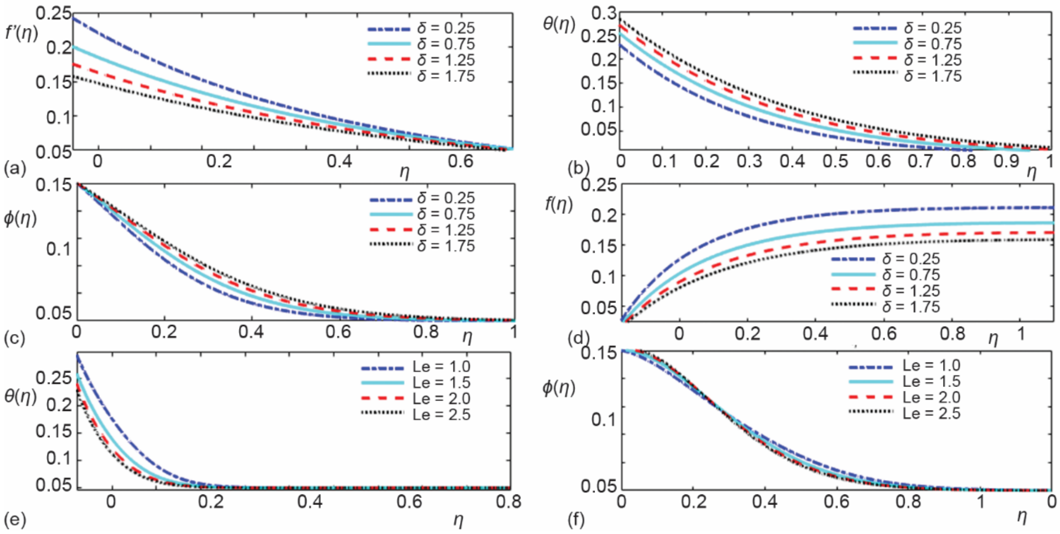

Figure 4. Impact of δ on f', θ, ϕ, and f while of Le on θ and ϕ; (a) f' for δ variation, (b) θ for δ variation, (c) ϕ for δ variation, (d) f for δ variation, (e) θ for Le variation, (f) ϕ for Le variation

The computed numerical data of local Nusselt number, Nt, are presented in tab. 2. It is seen that local Nusselt number grow by raising Nt, Le, and Pr while decay for δ, β, λ, Nc, and Sc, respectively. The numerical values of local Sherwood number are listed in tab. 3. The parameters Nc, Sc, and β enhanced while Nt, Le, Pr, δ, and λ diminish the local Sherwood number, respectively. The numerical values of skin friction coefficient are tabulated in tab. 5. The fluidic parameters δ enhance and λ reduce the skin friction. Table 4 is originated to narrate the numerical data of residual error acquired by proposed numerical approach during the numerical execution, which proved the higher accuracy obtained by this approach. Table 6 illuminated the numerical values of mesh points evaluated by proposed scheme for each fluidic sundry parameter. The numerically evaluated data of ODE and boundary conditions for every case of involved sundry fluidic parameter are portrayed in tabs. 7 and 8, respectively.

Concluding remarks

The effect of thermal and velocity slips conditions on flow of Williamson nanofluid past a stretching sheet are investigated numerically by employing the computation strength of Lobatto IIIA method. The outcomes of the presented nanofluidic Williamson model are provided as follows.

Table 3. Sherwood number analysis of proposed model

Index	C-1	C-2	C-3	C-4
δ	1.0835	0.9299	0.8373	0.7719
γ	0.5610	0.7585	0.8711	0.9439
λ	0.8544	0.8291	0.7946	0.7384
Pr	0.9057	0.8448	0.8015	0.7683
Nc	0.8376	0.8697	0.9015	0.9322
Le	0.1729	−0.1898	−0.1898	−0.2745
Nt	0.9156	0.5210	0.5210	0.4290
Sc	0.2248	0.9748	0.9748	1.2453

Table 4. Mesh points analysis of proposed model

Index	C-1	C-2	C-3	C-4
δ	971	945	1102	1078
γ	1193	1198	1198	958
λ	1198	1198	959	364
Pr	1998	1198	962	960
Nc	1998	1198	1198	913
Le	972	966	968	968
Nt	1114	1089	1045	1016
Sc	913	1198	1198	1198

Table 5. Skin friction analysis for proposed model

Index	C-1	C-2	C-3	C-4
δ	−0.6544	−0.4531	−0.3528	−0.2909
γ	−0.5327	−0.5327	−0.5327	−0.5327
λ	−0.5040	−0.5260	−0.5575	−0.6183
Pr	−0.5327	−0.5327	−0.5327	−0.5327
Nc	−0.5327	−0.5327	−0.5327	−0.5327
Le	−0.5327	−0.5327	−0.5327	−0.5327
Nt	−0.3961	−0.3961	−0.3961	−0.3961
Sc	−0.5327	−0.5327	−0.5327	−0.5327

Table 6. Relative error analysis of proposed model

Index	C-1	C-2	C-3	C-4
δ	$8.263\cdot10^{-15}$	$4.010\cdot10^{-15}$	$2.720\cdot10^{-15}$	$1.992\cdot10^{-15}$
γ	$3.630\cdot10^{-14}$	$7.247\cdot10^{-15}$	$6.354\cdot10^{-15}$	$5.783\cdot10^{-15}$
λ	$7.019\cdot10^{-15}$	$6.769\cdot10^{-15}$	$5.061\cdot10^{-14}$	$9.752\cdot10^{-13}$
Pr	$4.973\cdot10^{-15}$	$6.141\cdot10^{-15}$	$7.355\cdot10^{-15}$	$8.572\cdot10^{-15}$
Nc	$6.279\cdot10^{-15}$	$5.583\cdot10^{-15}$	$5.101\cdot10^{-15}$	$1.969\cdot10^{-14}$
Le	$2.788\cdot10^{-14}$	$5.204\cdot10^{-14}$	$5.990\cdot10^{-14}$	$6.195\cdot10^{-14}$
Nt	$3.510\cdot10^{-13}$	$3.962\cdot10^{-14}$	$1.921\cdot10^{-15}$	$2.515\cdot10^{-16}$
Sc	$5.403\cdot10^{-15}$	$5.090\cdot10^{-15}$	$9.028\cdot10^{-15}$	$1.557\cdot10^{-14}$

- The numerical results revealed that velocity profile decrease while temperature and concentration profiles enhance with an increment in slip parameter.
- The temperature θ and concentration ϕ profiles reduced with increase in the values of the Prandtl number.
- The increment in Williamson parameter leads to increased in both temperature and concentration profiles. Additionally, for larger Williamson parameter the boundary layer thickness increases.
- The temperature, θ, and concentration, ϕ, profiles decreased by enhancing values of thermal parameter.
- The proposed method provides better accuracy analysis through relative errors.
- The local Nusselt number grow up for Prandtl and Lewis numbers while reduced for varying values of velocity and thermal slip parameters.
- The local Sherwood number enhanced for thermal parameter and declined for velocity slip parameter.
- The local Skin friction declined for velocity slip parameter and increase by changing values of Williamson parameter.

In future, one may exploit intelligent computing paradigm for solving Williamson nanofluidic model.

Table 7. Numerical data of ODE for proposed model

Index	C-1	C-2	C-3	C-4
δ	37651	37157	35739	35283
γ	37468	37563	37563	37404
λ	37563	37563	35825	64637
Pr	37563	37563	37480	37442
Nc	37563	37563	37563	34951
Le	37670	37556	37594	37594
Nt	39570	39095	34657	34106
Sc	36549	37563	37563	37563

Table 8. Numerical data of boundary conditions for proposed model

Index	C-1	C-2	C-3	C-4
δ	120	120	98	97
γ	98	98	98	120
λ	98	98	118	189
Pr	98	98	120	120
Nc	98	98	98	118
Le	120	120	120	120
Nt	119	119	98	98
Sc	120	98	98	98

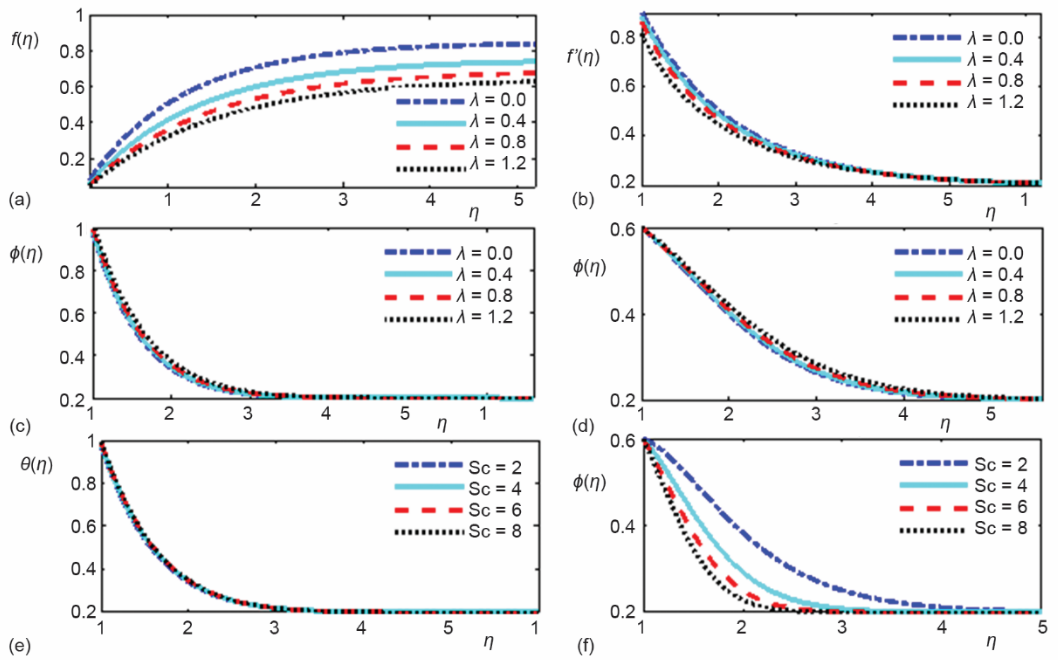

Figure 5. Impact of λ on f, f', θ, and ϕ while of Sc on θ and ϕ; (a) f for λ variation, (b) f' for λ variation, (c) θ for λ variation, (d) ϕ for λ variation, (e) θ for Sc variation, and (f) ϕ for Sc variation

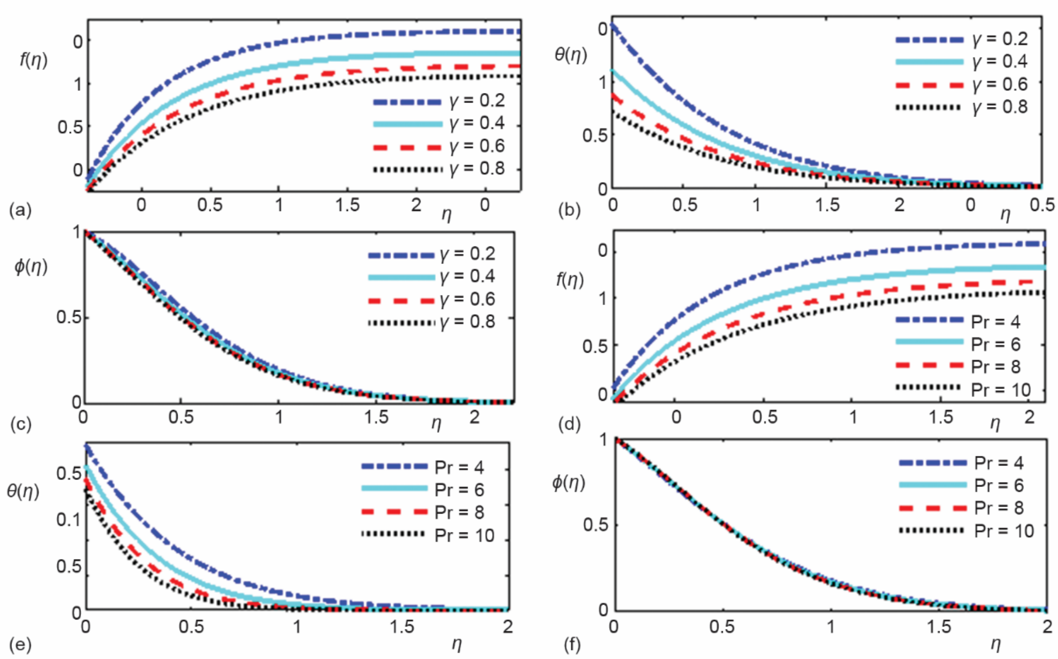

Figure 6. Impact of γ on f , θ and ϕ while of Pr on f , θ, and ϕ; (a) f for varying values of γ, (b) θ for γ variation, (c) ϕ for varying values of γ, (d) f for Pr variation, (e) θ for Pr variation, and (f) ϕ for Pr variation

References

[1] Bhatti, M. M., Rashidi, M. M., Effects of Thermo-Diffusion and Thermal Radiation on Williamson Nanofluid Over a Porous Shrinking/Stretching Sheet, *Journal of Molecular Liquids, 221* (2016), Sept., pp. 567-573

[2] Awais, M., *et al.*, Hydro-Magnetic Falkner-Skan Fluid Rheology with Heat Transfer Properties, *Thermal Science, 24* (2020), 1, pp. 339-346

[3] Saleem, S., *et al.*, Convective h#eat and # in magneto Walter's B Nanofluid Flow Induced by a Rotating Cone, *Arabian Journal for Science and Engineering, 44* (2019), 2, pp. 1515-1523

[4] Nadeem, S., Hussain, S., Flow and Heat Transfer Analysis of Williamson Nanofluid, *Applied Nanoscience, 4* (2014), 8, pp. 1005-1012

[5] Hamid, A., *et al.*, Numerical Simulation for Heat Transfer Performance in Unsteady Flow of Williamson Fluid Driven by a Wedge-Geometry, *Results in Physics, 9* (2018), June, pp. 479-485

[6] Rashid, M., *et al.*, Entropy Generation in Flow of Ferromagnetic Liquid With Non-Linear Radiation and Slip Condition, *Journal of Molecular Liquids, 276* (2019), Feb., pp. 441-452

[7] Ahmad, R., *et al.*, Numerical Study of MHD Nanofluid Flow and Heat Transfer Past a Bidirectional Exponentially Stretching Sheet, *Journal of Magnetism and Magnetic Materials, 407* (2016), June, pp. 69-74

[8] Bai, Y., *et al.*, Stagnation-Point Heat and Mass Transfer of MHD Maxwell Nanofluids Over a Stretching Surface in the Presence of Thermophoresis, *Journal of Molecular Liquids, 224* (2016), Dec., pp. 1172-1180

[9] Shehzad, S. A., *et al.*, Non-Linear Thermal Radiation in Three-Dimensional Flow of Jeffrey Nanofluid: A Model for Solar Energy, *Applied Mathematics and Computation, 248* (2014), Dec., pp. 273-286

[10] Ibrahim, W., Magnetohydrodynamic (MHD) Boundary Layer Stagnation Point Flow and Heat Transfer of a Nanofluid Past a Stretching Sheet with Melting, *Propulsion and Power Research, 6* (2017), 3, pp. 214-222

[11] Reddy, S., *et al.*, MHD Flow and Heat Transfer Characteristics of Williamson Nanofluid Over a Stretching Sheet with Variable Thickness and Variable Thermal Conductivity, *Transactions of A. Razmadze Mathematical Institute, 171* (2017), 2, pp. 195-211
[12] Soomro, F. A., Heat Generation/Absorption and Non-Linear Radiation Effects on Stagnation Point Flow of Nanofluid Along a Moving Surface, *Results in physics, 8* (2018), Mar., pp. 404-414
[13] Prasannakumara, B., MHD Flow and Non-Linear Radiative Heat Transfer of Sisko Nanofluid Over a Non-Linear Stretching Sheet, *Informatics in Medicine Unlocked, 9* (2017), C, pp. 123-132
[14] Alam, M., *et al.*, Solution of Falkner-Skan Unsteady MHD Boundary Layer Flow and Heat Transfer Past a Moving Porous Wedge in a Nanofluid, *Procedia engineering, 194* (2017), Sept., pp. 414-420
[15] Bellen, A., *et al.*, Methods for Linear Systems of Circuit Delay Differential Equations of Neutral Type, *IEEE Transactions on Circuits and Systems I: Fundamental Theory and Applications, 46* (1999), 1, pp. 212-215
[16] Ryland, B. N., McLachlan, R. I., On Multisymplecticity of Partitioned Runge-Kutta Methods, *SIAM Journal on Scientific Computing, 30* (2008), 3, pp. 1318-1340
[17] Uddin, I., *et al.*, Numerical Treatment for Fluidic System of Activation Energy with Non-Linear Mixed Convective and Radiative Flow of Magneto Nanomaterials with Navier's Velocity Slip, *AIP Advances, 9* (2019), 5, ID 055210
[18] Nagoor, A. H., *et al.*, Numerical Treatment for Three-Dimensional Rotating Flow of Carbon Nanotubes with Darcy-Forchheimer Medium by the Lobatto IIIA Technique, *AIP Advances, 10* (2020), 2, ID 025016
[19] Ahmad, I., *et al.*, A Novel Application of Lobatto IIIA Solver for Numerical Treatment of Mixed Convection Nanofluidic Model, *Scientific Reports, 11* (2021), 1, pp. 1-16
[20] Shoaib, M., *et al.*, Numerical Analysis of 3-D MHD Hybrid Nanofluid Over a Rotational Disk in Presence of Thermal Radiation with Joule Heating and Viscous Dissipation Effects Using Lobatto IIIA Technique, *Alexandria Engineering Journal, 60* (2021), 4, pp. 3605-3619
[21] Lund, L. A., *et al.*, Darcy-Forchheimer Porous Medium Effect on Rotating Hybrid Nanofluid on a Linear Shrinking/Stretching Sheet, *International Journal of Numerical Methods for Heat & Fluid Flow*, On-line first, https://doi.org/10.1108/NFF-11-2020-0716, 2021
[22] Vucheva, V., Kolkovska, N., High Order Symplectic Finite Difference Scheme for Double Dispersion Equations, *AIP Conference Proceedings, 2321*, (2021), 1, 030037
[23] Versaci, M., *et al.*, Micropumps for Drug Delivery Systems: A New Semi-Linear Elliptic Boundary-Value Problem, *Computational and Applied Mathematics, 40* (2021), 2, pp. 1-21
[24] Shampine, L. F., *et al.*, Solving Boundary Value Problems for Ordinary Differential Equations in Matlab With BVP4C, *Tutorial notes, 2000* (2000), Oct., pp. 1-27

Paper submitted: June 20, 2020
Paper revised: March 20, 2021
Paper accepted: April 3, 2021